# Macroscopic framework for visco- and poroelasticity and wave-induced flow – Part II: Effective Media

Igor B. Morozov and Wubing Deng
University of Saskatchewan, Saskatoon, Saskatchewan, CANADA, E-mails:
igor.morozov@usask.ca, wubing.deng@usask.ca

## *Abstract*

Many wave-propagating media important for seismic exploration support secondary P waves. The most important types of such media are porous rocks with wave-induced fluid flows. Although difficult to isolate, secondary waves produce significant effects in the presence of any heterogeneity, such as for predicting the seismic reflectivity and empirical moduli measured in rock samples in the laboratory. The conventional concept of the viscoelastic modulus does not account for secondary waves, but the General Linear Solid (GLS) framework described in Part I of this paper yields a consistent and rigorous approach. In the present Part II, this approach is applied to two types of effective media. First, for a rock consisting of alternating thin sandstone layers saturated with brine and gas, the effective medium exhibits not only viscoelastic (viscosity) both also fluid-friction (Darcy) properties. The effective-medium model predicts the velocity dispersion and attenuation for both the primary and secondary waves. Effective-medium relations can be derived in a (relatively) closed form for the density and elasticity, but not for the parameters of internal friction. Notably, the effective elastic bulk modulus (responsible for low-frequency P-wave velocity) is significantly lower than the lower-bound (Reuss) average of the moduli of the constituent rocks. In the second example, a Generalized Standard Linear Solid effective medium is considered. This model is broadly used for modeling attenuation in seismic waveform simulation software. From the GLS point of view, some (petro)physical significance should be allowed for the internal (such as memory) variables. Inertial effects and interactions between these internal variables cause secondary wave modes with variable dispersion characteristics. Overall, to explain the wave propagation and reflections in heterogeneous media, realistic effective-medium models need to account for both the primary and secondary wave modes and also for both viscous- and fluid-friction effects.

## *Introduction*

In Part I of this study (Morozov and Deng, submitted to Geophysics), we described a common framework for describing the linear viscoelasticity, poroelasticity, and macroscopic wave-induced fluid flows (WIFF). The approach is based on Lagrangian formulation of continuum mechanics, which is well known in theoretical physics (Landau and Lifshitz, 1986) and formed the basis of Biot's (1962) poroelasticity. The framework, which we call the General Linear Solid (GLS), describes the mechanical properties of the medium by a minimal set of 'observable' and 'internal' macroscopic variables, which are governed only by the fundamental principles of energy, linearity, and symmetry. The specific choices of the variables, the character of their interaction, and the properties of energy functions involved needs to be determined from the specific physical mechanisms. These mechanisms are determined at the microscopic or mesoscopic scales and depend on the character of mineral assemblage, granular structure, porosity, fracturing of the rock, presence of fluids, etc.. In the present Part II, we focus on applying the GLS approach for constructing effective (i.e., macroscopically-averaged) media.

Practical seismology is mostly interested in heterogeneous media and bodies of finite dimensions, such as layered rock sequences in the field or small rock samples measured in the lab. When approaching a heterogeneous medium, it is important to first consider the question whether the conventional description of its mechanical properties by a pair of constitutive parameters (*density + effective viscoelastic modulus*) is sufficient and accurate. As shown in Part I, for poroelastic and likely most WIFF media, the answer to this question is negative. The reliance on the moduli leads to quantitatively incorrect predictions of reflectivity within layered poroelastic media. The Darcy-type friction is fundamentally different from both viscosity and elasticity (as a body force differs from a divergence of stress), and these mechanisms lead to different properties of reflectivity. In a layered poroelastic rock, P-wave reflections result from interactions of *two* waves (primary and secondary, Biot's), which cannot be modeled by a single viscoelastic modulus. Dutta and Odé (1979a) showed that such secondary waves also exist in effective WIFF media with patchy saturation. Similarly, both the primary and secondary modes contribute to the dynamic moduli measured in small samples in the lab (Morozov, submitted to *Geophysics*).

To further emphasize the role of heterogeneity, note that poroelasticity represents an effective-medium model, in which an elastic rock is mixed with a fluid that is elastic with respect to bulk deformation and viscous with respect to shear. Despite both of these constituents being purely viscoelastic (i. e. described by complex-valued moduli), the resulting effective medium exhibits Darcy friction but no viscosity (Biot, 1962). This suggests that Darcy-type friction may naturally arise when multiple constituents are combined to form an effective medium. In such cases, the simple viscoelastic (*density + modulus*) approximation should be insufficient. Nevertheless, the more general GLS model contains all isotropic linear cases (with the usual assumption about decoupled

shear and bulk deformations; Part I).

In the present Part II, we extend the GLS concept to effective media. The approach is based on the idea that *all four* constitutive properties (*density*, *modulus*, *solid viscosity*, and *Darcy friction*) become "effective", i.e. averaged when multiple constituents are replaced with a macroscopically-uniform effective medium. Each of these properties is represented by a matrix, and therefore the resulting model is substantially more multivariate and complex, but also more complete and accurate than the viscoelastic approximation. An additional nontrivial question arises about the number of degrees of freedom (internal variables) necessary for an adequate description of the effective medium. At the same time, the constitutive properties of the GLS contain no time/frequency dependences, which is much simpler than the viscoelastic moduli (Part I).

The key observation of this paper is that because most realistic physical models of wave propagation contain secondary P waves (such as diffusive, fluid, or inhomogeneous), these waves must be important when modeling heterogeneous media, i.e. for practically all cases of interest. Even though the secondary waves may be difficult to isolate experimentally, they nevertheless contribute to reflectivity and measurements with small samples in the lab (Part I; Morozov, submitted to Geophysics). Consequently, successful effective-media models should reproduce not only the primary mode but also a sufficient number of secondary modes. This can be achieved by using the GLS formulation with the total number of variables $N > 1$. To illustrate such effective media quantitatively, we consider two groups of models:

1) Effective media produced by fine layering of poroelastic materials (Part I); and
2) Effective media extending the concept of the Generalized Standard Linear Solid (GSLS; Lakes, 2009).

The first of these models is often used as a simple example of WIFF (White, 1975; Gurevich et al., 1997). As mentioned above, if this model is intended, for example, for predicting seismic reflectivity, it cannot be limited to a reproducing a frequency-dependent effective modulus but should be of the more general "poro-viscoelastic" type (Part I).

The second model above (GSLS) is broadly used to explain the band-limited, near-constant $Q^{-1}(f)$ observed within the Earth (Liu et al., 1976) and to implement attenuation in seismic waveform simulation software (*e.g.*, Zhu et al., 2013). An attractive feature of this model is its ability to simulate seismic wave attenuation without considering its mechanisms, which are replaced by constructing a sufficiently complex GSLS. However, is this replacement always adequate? In the time domain, modeling a GSLS-type medium is implemented by a set of internal or "memory" variables (*ibid*), and therefore, the GSLS represents a special case of the GLS (see Part I). However, the GLS point of view also suggests that the physical meanings of these mathematical variables can (and apparently should) still be considered. Once some physical significance is allowed for the internal variables, it becomes necessary to also consider the possible

inertial effects and interactions associated with these variables. The presence of inertial effects would lead to more complex wavefields containing additional wave modes analogous to Biot's waves in fluid-saturated porous rocks. As above, the secondary wave modes should likely be nt seen in uniform media but important for modeling reflections and transmissions on heterogeneities, *i.e.* in practically all cases of interest in exploration seismology.

### *Effective GLS media*

The mechanical properties of a GLS medium are described by six constitutive matrix properties $\boldsymbol{\rho}$, $\mathbf{K}$, $\boldsymbol{\mu}$, $\boldsymbol{\eta}_K$, $\boldsymbol{\eta}_\mu$, and $\mathbf{d}$, which are the density, bulk and shear elasticity, bulk and shear viscosity, and Darcy's friction, respectively. As shown in Part I, by setting some of these matrices equal zero, we obtain the elastic solid, Stokean or Newtonian viscous fluid, all types of viscoelastic solids, and Biot's (1962) saturated porous solid. These matrices form the Lagrangian ($L$) and dissipation function ($D$) densities (equations 5 and 6 in Part I):

$$\begin{cases} L = \frac{1}{2}\dot{\mathbf{u}}_i^T \boldsymbol{\rho} \dot{\mathbf{u}}_i - \frac{1}{2}\boldsymbol{\Delta}^T \mathbf{K} \boldsymbol{\Delta} - \tilde{\boldsymbol{\varepsilon}}_{ij}^T \boldsymbol{\mu} \tilde{\boldsymbol{\varepsilon}}_{ij}, \\ D = \frac{1}{2}\dot{\mathbf{u}}_i^T \mathbf{d} \dot{\mathbf{u}}_i + \frac{1}{2}\dot{\boldsymbol{\Delta}}^T \boldsymbol{\eta}_K \dot{\boldsymbol{\Delta}} + \dot{\tilde{\boldsymbol{\varepsilon}}}_{ij}^T \boldsymbol{\eta}_\mu \dot{\tilde{\boldsymbol{\varepsilon}}}_{ij}, \end{cases} \tag{1}$$

where $\mathbf{u}$ is the hitherto arbitrary displacement field including both the observable deformation and internal variables such as the pore-fluid displacement in poroelasticity, and $\boldsymbol{\Delta}$ and $\boldsymbol{\varepsilon}$ are the corresponding strains. Let us denote the number of components in $\mathbf{u}$ by $N$.

As shown in Part I, the connection between the physical properties of the medium and the dispersion and attenuation of a wave in it lies in the following generalized eigenvector problem (equation 19 in Part I):

$$\left(\boldsymbol{\rho} + \frac{i}{\omega}\mathbf{d}\right)\boldsymbol{\upsilon}^{(n)} = \gamma\left(\mathbf{M} - i\omega\boldsymbol{\eta}_M\right)\boldsymbol{\upsilon}^{(n)}, \tag{2}$$

where $\omega$ is the wave frequency, and $\mathbf{M}$ and $\boldsymbol{\eta}_M$ denote some appropriate combinations of the elastic moduli and viscosities, such as the P-wave modulus. The complex eigenvalue $\gamma$ contains the phase velocity and attenuation: $V_{\text{phase}}^* \equiv \omega / k^* = 1 / \operatorname{Re}\sqrt{\gamma}$ ,and eigenvector $\boldsymbol{\upsilon}^{(n)}$ contains the information about the internal polarization of the $n^{\text{th}}$ mode (generally, $n = 1 \ldots N$).

In a micro- or mesoscopically heterogeneous medium, the displacements, strains, and consequently functions $L$ and $D$ are highly spatially heterogeneous. Functional derivatives of $L$ and $D$ in equations 1 completely determine the dynamics of the system (Part I). For the kinetic and elastic-energy terms in relations 1, these derivatives can be evaluated independently of the other terms. Consequently, when replacing a heterogeneous medium with an effective one (uniform at scales shorter than the

macroscopic wavelength), we must ensure that these terms in the functional forms 1 are preserved for the appropriate deformation:

$$\dot{\underline{\boldsymbol{\Delta}}}^T \underline{\boldsymbol{\rho}} \dot{\underline{\boldsymbol{\Delta}}} = \dot{\boldsymbol{\Delta}}^T \boldsymbol{\rho} \dot{\boldsymbol{\Delta}} \,,\ \underline{\boldsymbol{\Delta}}^T \underline{\mathbf{K}} \underline{\boldsymbol{\Delta}} = \boldsymbol{\Delta}^T \mathbf{K} \boldsymbol{\Delta} \text{ , and } \underline{\tilde{\boldsymbol{\varepsilon}}}_{ij}^T \underline{\boldsymbol{\mu}} \underline{\tilde{\boldsymbol{\varepsilon}}}_{ij} = \tilde{\boldsymbol{\varepsilon}}_{ij}^T \boldsymbol{\mu} \tilde{\boldsymbol{\varepsilon}}_{ij} \,, \tag{3}$$

where the underbars indicate the quantities in the smoothed effective medium. Equations 3 can be described as "homogenization" of the medium. Clearly, if these equations can be satisfied for any deformation by choosing the appropriate $\underline{\boldsymbol{\rho}}$, $\underline{\mathbf{K}}$, and $\underline{\boldsymbol{\mu}}$, the macroscopic behavior of the effective medium would be identical to that of the original medium. However, with regard to the frictional parameters $\underline{\mathbf{d}}$, $\underline{\boldsymbol{\eta}}_K$, and $\underline{\boldsymbol{\eta}}_\mu$, the situation is more difficult, as discussed below.

**Number of degrees of freedom**

The parameter matrices $\underline{\boldsymbol{\rho}}$, $\underline{\mathbf{K}}$, and other should contain sufficient numbers of rows and columns to represent the relevant degrees of freedom in the effective medium. This number of degrees of freedom depends on the microstructure and can be variable and difficult to determine. For example, within porous saturated rock, both the solid and fluid phases have $N = 1$ and can deform independently. Consequently, the effective poroelastic medium contains $N = 2$ degrees of freedom and supports two P-wave modes. Similarly, in a porous rock with two types of patchy saturation (for example, oil and brine), each of the phases has $N = 2$ and generally, we can expect $N = 4$ and four P-wave modes in the effective medium. However, if there exists a distinct boundary between the two phases, such as in subsection *Wave-induced fluid flow (WIFF)* below, the number of resulting modes reduces to $N = 2$. If the solid frame can be treated as uniform and the two constituents of the mix only differ by saturation with different fluids, then we would have $N = 3$.

For a tractable description of an effective medium, we need to approximate it with lower number of degrees of freedom. The acceptable value of $N$ can probably be judged by the number of wave modes with significant amplitudes generated on boundaries and heterogeneities. For example, if we are only interested in wave propagation in a uniform medium, than a single P-wave mode (the fastest and lowest-attenuation) could be sufficient, and consequently we could use $N = 1$. This is the conventional approach using the *scalar* effective modulus and density. However, if reflections are of interest, the second, 'slow' mode is significant near the reflectors and free boundaries (Part I). In such cases, $N = 2$ appears to be the necessary minimum.

Thus, we argue that in order to be realistic, the effective medium containing pore fluids must support at least two P-wave modes. This means that the kinetic, elastic, and dissipation properties of the effective medium must be represented by 2×2 GLS matrices.

**Homogenization relations for ρ and K**

Homogenization relations for effective media, such as the Gassman's fluid

substitution law or Terzaghi's principle, require certain models of the microstructure and specific meanings of the field variables $\mathbf{u}$. In the GLS model, the derivation of the homogenization equations for density ($\boldsymbol{\rho}$) and bulk modulus ($\mathbf{K}$) can be made by considering several independent types of deformations (even hypothetical) applied to the material and requiring that the effective medium reproduces the kinetic and elastic energies of all these deformations. If such a replacement can be achieved, all macroscopic equations of motion (arising entirely from the energy forms 1; Part I) will correctly reproduce the propagation of long waves in the original medium. As shown in Appendix A, for poroelasticity, this approaches yields the equations for the 2×2 density matrix, bulk rigidity matrix, and Gassmann's fluid substitution equations (Bourbié *et al*., 1987).

Consider a mixture of $N_m$ poroelastic materials each having $N = 2$ and obeying GLS relations 1. We will replace them with a smooth effective medium also obeying the same relations. The distribution of the mixed media can be heterogeneous and 'patchy' on the microscopic or mesoscopic scales, i.e. short compared to the shortest wavelength. As in a 1-D numerical example in the next section, let us assume that each of these materials occupies a certain volume fraction $f_j$ of the rock (where $j = 1..N_m$ is the number of the material) and is in equilibrium with adjacent areas. These requirements reduce the number of degrees of freedom in the effective medium to $N = 2$.

Let us denote $\mathbf{u}^j$ the displacement of the $j^{\text{th}}$ constituent of the compound and $\underline{\mathbf{u}}$ the locally-constant average displacement of the effective medium. The difference between these displacements: $\mathbf{u}' \equiv \mathbf{u}^j - \underline{\mathbf{u}}$ is quickly variable in space with zero mean: $\langle \mathbf{u}' \rangle = 0$. To determine the effective density, let us conduct a thought experiment by deforming the body with an arbitrary and macroscopic rate $\dot{\underline{\mathbf{u}}}$. The average kinetic energy (in relation 1) is:

$$\langle E_{kin} \rangle = \frac{1}{2} \left\langle \dot{\mathbf{u}}_i^T \boldsymbol{\rho} \dot{\mathbf{u}}_i \right\rangle = \frac{1}{2} \dot{\underline{\mathbf{u}}}_i^T \langle \boldsymbol{\rho} \rangle \dot{\underline{\mathbf{u}}}_i + \frac{1}{2} \left\langle \dot{\mathbf{u}}_i'^T \boldsymbol{\rho} \dot{\mathbf{u}}_i' \right\rangle . \tag{4}$$

The local spatial average of the density in the first term in this expression is the Voigt average of the densities of the constituents:

$$\langle \boldsymbol{\rho} \rangle = \sum_{j=1}^{N_m} f_j \boldsymbol{\rho}^j . \tag{5}$$

The second term in expression 4 is more difficult to evaluate, but its general character can be understood from an analogy with poroelasticity. If the deformation of the medium involves fluid flowing around micro- or mesoscopic heterogeneities (such as the grains formed by the constituents), the average flow velocity will be proportional to $\dot{\underline{\mathbf{u}}}$. This can be written as $\left\langle \dot{\mathbf{u}}_i'^T \dot{\mathbf{u}}_i' \right\rangle = (a-1) \dot{\underline{\mathbf{u}}}^T \dot{\underline{\mathbf{u}}}$, where $a$ is analogous to the tortuosity of the pore space (Appendix A). Therefore, the second term in expression 4 can be written as

$\left\langle \dot{\mathbf{u}}_i'^T \boldsymbol{\rho} \dot{\mathbf{u}}_i' \right\rangle = \underline{\dot{\mathbf{u}}}_i^T \boldsymbol{\rho}_a \underline{\dot{\mathbf{u}}}_i$, where $\boldsymbol{\rho}_a$ is the contribution to the effective density from the tortuosity of the mesoscopic flow. This matrix depends on the structure of the compound and is likely very difficult to determine analytically. At the same time, numerical modeling of this quantity appears relatively straightforward.

For an arbitrary $\underline{\dot{\mathbf{u}}}$, the expression 4 should equal the kinetic energy of the effective medium: $\langle E_{kin} \rangle = \left( \underline{\dot{\mathbf{u}}}_i^T \underline{\boldsymbol{\rho}} \underline{\dot{\mathbf{u}}}_i \right) / 2$ . Therefore, the effective density equals:

$$\underline{\boldsymbol{\rho}} = \sum_{j=1}^{N_m} f_j \boldsymbol{\rho}^j + \boldsymbol{\rho}_a \,. \tag{6}$$

The difference of the effective density $\underline{\boldsymbol{\rho}}$ from the simple average $\sum_{j=1}^{N_m} f_j \boldsymbol{\rho}^j$ is similar to poroelasticity, in which the relative movement of pore fluids modifies the effective density experienced within a wave from $\rho$ to $\rho + (a-1)\rho_f$, where $\rho_f$ is the density of the pore fluid and *a* is the tortuosity (Bourbié *et al.,* 1987, p.71; also see Appendix A).

To determine the (matrix) effective bulk modulus, we use the parameterization from poroelasticity (equation 29 in Part I; Bourbié *et al.,* 1987):

$$\underline{\mathbf{K}} = \begin{bmatrix} \underline{K}_f & -\underline{\beta}\underline{M} \\ -\underline{\beta}\underline{M} & \underline{M} \end{bmatrix} \,. \tag{7}$$

As shown in Appendix A, the three parameters $\underline{K}_f$, $\underline{M}$, and $\underline{\beta}$ in this expression can be determined by considering three different shapes of static deformations and equating the elastic energies of the small-scale structure and effective medium. Such deformations can be selected as (Appendix A): 1) a closed-system compression with zero fluid flow; 2) an open-system deformation with empty pores; and 3) a compression with zero effective pressure. The effective modulus $\underline{K}_f$ is the "wet" rock modulus measured in the first of these experiments. This modulus should be related to the corresponding modulus of the constituent materials by some type of average depending on the geometry and other properties of the grains. We use the following generalized average:

$$\underline{K}_f = \alpha \left[ \sum_{j=1}^{N_m} f_j \, K_f^{-1} \Big|_j \right]^{-1} \,. \tag{8}$$

With $\alpha = 1$, this is the Reuss average that should be appropriate an iso-stress model of the compound similar to that in the next section. However, as illustrated in the section *Examples*, the effective $\underline{K}_f$ also depends on the boundary conditions between the constituents, and the lower-bound average 8 still overestimates the $\underline{K}_f$ . To compensate this overestimation, we use an empirical factor $\alpha$. The dry effective modulus and the

effective modulus of the fluid can similarly be approximated by Reuss averages:

$$\underline{K}_0^{-1} = \sum_{j=1}^{N_m} f_j \, K_0^{-1}\Big|_j \text{ and } \underline{K}_{fl}^{-1} = \sum_{j=1}^{N_m} f_j \, K_{fl}^{-1}\Big|_j . \tag{9}$$

The parameters $\underline{\beta}$ and $\underline{M}$ in matrix 7 can be obtained from these averages by using relations inferred from the above three experiments with the compound medium (Appendix A):

$$\underline{\beta} = 1 - \underline{K}_0 / \underline{K}_s , \tag{10}$$

$$\underline{\beta}^2 \underline{M} = \underline{K}_0 - \underline{K}_f . \tag{11}$$

**Homogenization of internal friction**

Apparently no homogenization equations similar to those for $\underline{\boldsymbol{\rho}}$ and $\underline{\mathbf{K}}$ in the preceding section can be derived for the effective internal-friction matrices $\underline{\boldsymbol{\eta}}_K$ and $\underline{\mathbf{d}}$ in the effective media. Note that the closed-form equations for $\underline{\boldsymbol{\rho}}$ and $\underline{\mathbf{K}}$ above are possible because there exist deformations sensitive to only kinematic or elastic effects. By contrast, in any deformation of a heterogeneous medium, the effects of $\boldsymbol{\eta}$ and $\mathbf{d}$ are always coupled among themselves and also with those of the density and elasticity. Therefore, for example, the effective viscosity $\underline{\boldsymbol{\eta}}_K$ would also contain contributions from $\mathbf{d}$ and $\mathbf{K}$, and also depend on the form of the deformation. These observations differ from the conventional viscoelasticity, in which it is *assumed* that the dynamic (frequency-dependent) moduli obey all relations for the elastic moduli, including the homogenization relations (Makarynska et al., 2010; Mavko, 2013).

If $\mathbf{d} \equiv \mathbf{0}$ (in which case the GLS is a linear, purely viscoelastic medium, the effective viscosity matrix can be constructed from the correspondence principle (Part I). The elastic and viscous responses for both the original and effective media can be combined in a symmetric 2×2 matrices $\mathbf{K}^* \equiv \mathbf{K} - i\omega\boldsymbol{\eta}_K$. It appears reasonable to speculate that the corresponding viscosity parameters can also be incorporated in the observable moduli $K_f$, $K_0$, and $K_{fl}$ in equations 8-11, and complex-valued parameters $\underline{K}_f^*$, $\underline{\beta}^*$ and $\underline{M}^*$ can be evaluated from them. Then, the effective complex modulus becomes, similar to equation 7:

$$\underline{\mathbf{K}} - i\omega\underline{\boldsymbol{\eta}}_K = \begin{bmatrix} \underline{K}_f^* & -\underline{\beta}^* \underline{M}^* \\ -\underline{\beta}^* \underline{M}^* & \underline{M}^* \end{bmatrix}. \tag{12}$$

As the effective elastic modulus $\underline{\mathbf{K}}$ is given by equation 7, $\underline{\boldsymbol{\eta}}_K$ can be found from this

relation. However, this derivation is still strongly limited, because it makes $\underline{\boldsymbol{\eta}}_K$ frequency-dependent and is only valid under two approximations: 1) linearity of viscosity, and 2) absence of Darcy friction. Both of these approximations are likely violated in practical cases.

Because of the above difficulty of finding the effective parameter matrices $\boldsymbol{\eta}$ and $\mathbf{d}$ for realistic cases, we propose deriving them empirically, by fitting the frequency-dependent velocity dispersion and attenuation for the available wave modes. This approach is illustrated on the first numerical example in the following section.

## *Examples*

### Wave-induced fluid flow (WIFF)

WIFF effects occur in a medium containing 'mesoscale' heterogeneities with contrasting pore-fluid contents, such as brine and gas. Upon passage of a seismic wave, fluid flows between these heterogeneities cause characteristic, often lower-frequency and higher-magnitude peaks in the wave-energy dissipation. White (1975) modeled such effects in a spherical gas-saturated rock enclosed in a spherical brine-saturated shell. This model was later improved by Dutta and Odé (1979a) and used in many recent studies (*e.g.*, Carcione and Piccotti, 2006; Müller et al, 2010). We also consider this example in one dimension, in an infinite sequence of plane, alternating gas- and water-saturated layers oriented orthogonally to the direction of P-wave propagation (Figure 1). Each layer is governed by the equations of poroelasticity, which means a GLS with $N = 2$, $\boldsymbol{\eta} \equiv 0$, and constitutive matrices $\boldsymbol{\rho}$, $\mathbf{K}$, and $\mathbf{d}$ given in Part I. Layer thicknesses $H_i$ and $H_2$ are considered small compared with the wavelength. Layered stochastic models of such kind were studied by Gurevich et al. (1997), who approximately separated the poroelastic, scattering, and fluid-flow effects. We give an exact, numerical solution to this problem, which can also be readily applied to a more complex and random layering.

Using the propagator method for poroelastic layering described in Part I, the wavefield in any layer can be related to those in the adjacent layers. We denote the wavefield at the rear boundary of each layer by a four-component vector $\mathbf{q}_r = \left(A_1^+ \quad A_2^+ \quad A_1^- \quad A_2^-\right)^T$, where the subscripts $J = 1,\ 2$ of the amplitudes $A_J^{\pm}$ correspond to the variables of the poroelastic displacement, and superscripts '$^+$'and '$^-$' denote the wave modes in equation 2 propagating forward and backward, respectively. Using this vector in layer $j$, the wavefield in the next layer can be expressed as

$$\mathbf{q}_r^{j+1} = \mathbf{S}^j \mathbf{q}_r^j, \tag{13}$$

where $\mathbf{S}^j \equiv \left(\mathbf{B}^{j+1}\right)^{-1} \mathbf{B}^j \mathbf{P}^j$ , $\mathbf{P}^j$ is the propagator matrix within the layer (equation 38 in Part I), and matrix $\mathbf{B}^j$ expresses the boundary condition between layers $j$ and $j$+1 (equation 41 in Part I). By applying this procedure across two layers, we obtain a relation between the fields in the first and third layers:

$$\mathbf{q}_r^3 = \hat{\mathbf{P}}^{13}\mathbf{q}_r^1, \tag{14}$$

where $\hat{\mathbf{P}}^{13} \equiv \mathbf{S}^2\mathbf{S}^1$. Because of the periodicity of the structure, the amplitudes within layer 3 are proportional to those in layer 1:

$$\mathbf{q}_r^3 = \lambda\mathbf{q}_r^1, \tag{15}$$

which means that $\lambda$ is an eigenvalue of matrix $\hat{\mathbf{P}}^{13}$. Macroscopically (when averaged over scale lengths much longer than the thicknesses of the layers but shorter than the wavelength), this wavefield represents a harmonic wave with exponentially decaying amplitude. The eigenvalue $\lambda$ can be written as $\lambda = \exp\left[ik^*\left(H_1 + H_2\right)\right]$, where $k^*$ is the complex wavenumber of the macroscopic wave: $k^* = \left(\omega/V_{\text{phase}}\right)\left(1 + iQ^{-1}/2\right)$. Therefore, propagation parameters for the effective wave equal:

$$k^* = \frac{-i\ln\lambda}{H_1 + H_2},\ V_{\text{phase}} = \frac{\omega}{\text{Re}\,k^*},\ \text{and}\ Q^{-1} = \frac{2\,\text{Im}\,k^*}{\text{Re}\,k^*}. \tag{16}$$

With $N = 2$, the 4×4 matrix $\hat{\mathbf{P}}^{13}$ has four eigenvalues corresponding to the 'fast' (primary) and 'slow' (secondary) waves traveling in two directions of axis $X$. For a stack of alternating brine- and gas-saturated layers of 1-cm thickness, with parameters given in Table 1, the velocities and attenuation factors of these waves calculated from relations 15 and 16 are shown in Figure 2. The calculations in this Figure were conducted up to the frequencies at which the slow-mode wavelengths became short enough to cause aliasing when evaluating the wavenumber 16. This restriction of the frequency agrees with the approximation of small-scale layering adopted in this modeling.

As expected, the effective medium generally behaves as a poroelastic one, with the primary ('fast') P wave having a near-constant velocity of about 1460 m/s to about 3-kHz frequency, after which the velocity increases (Figure 2a). These frequencies correspond to the position of the poroelastic effect in gas-saturated sandstone (Figure 5 in Part I). The slow effective wave emerges at lower frequencies of ~100 Hz (Figure 2a). Note that the increase in the 'slow'-wave velocity occurs at significantly lower frequencies than the dispersion of the 'fast' effective wave, and at the same frequencies, the attenuation of the 'fast' wave increases. Both of these increases affect seismic reflections (Part I). The 'slow' wave in the effective medium is diffusive above ~1 kHz, where its $Q < 1$ (Figure 2b).

Note that both the 'fast' and 'slow' effective P waves contain all four forward- and backward-directed modes within the brine- and gas-saturated layers. Figure 3 shows the amplitudes of these modes relative to the rock displacement (component $u_1$) of the effective wave. For the 'fast' effective wave (Figure 3a), the relative fluid motion (component $u_2$) within these modes increases with frequency, whereas in the 'slow' effective wave, the fluid motion decreases with frequency (Figure 3b).

Notably, even the lower-bound estimate for $\underline{K}_f$ given by relation 8 with $\alpha$=1 significantly overpredicts the primary P wave velocity at low frequencies (about 1687 m/s compared with the actual 1459 m/s; Figure 2a). For comparable thicknesses of the gas- and brine-saturated layers, the effective velocity is near constant (Figure 4a) despite the variable values of $\underline{K}_f$. The correction factor $\alpha$ in relation 8 is therefore below one and near-linearly increases when the relative thickness of the gas-saturated layers $f_{\text{gas}}$ exceeds about 0.1 (Figure 4b). The above effects occur because the pore fluids flow between the brine- and gas-saturated layers in this model (note that this is similar to the previously discussed models, such as by White (1975 and Dutta and Odé (1979a,b)). If the layers are insulated so that the pore fluids do not cross their boundaries (the second boundary condition shown in the inset of Figure 1), then a similar modeling (Appendix B) shows that the velocity at low frequencies is correctly predicted by the Reuss average of the modulus 7, with $\alpha = 1$ (Figure 2a). The attenuation is extremely low this case, because the pore fluids are effectively "frozen" by the zero-displacement boundary conditions on both boundaries of each layer.

To evaluate the parameters of internal friction, we use a simple Monte-Carlo search method to fit both the velocity dispersion and $Q^{-1}$ curves for both wave modes. The effective density is taken in the form 5 and the effective bulk modulus in the form 7, with parameter $\alpha = 0.63$ (Figure 4b) selected to satisfy the velocity limit at low frequencies (Figure 2a). As in poroelasticity, the effective Darcy friction matrix is taken in the form:

$$\underline{\mathbf{d}} = \begin{bmatrix} 0 & 0 \\ 0 & d \end{bmatrix}. \tag{17}$$

where the variable $d$ is randomly drawn from the interval $[0, 2\eta_{\text{brine}}/\kappa]$,where the viscosity of pore brine $\eta_{\text{brine}}$ and the permeability $\kappa$ are given in Table 1. The solid bulk viscosity matrix is taken in the form

$$\underline{\boldsymbol{\eta}}_K = \begin{bmatrix} \eta_1 & -\eta_3 \\ -\eta_3 & \eta_2 \end{bmatrix}, \tag{18}$$

where $\eta_1$, $\eta_2$,and $\eta_3$ are randomly drawn from the interval $\left[0, 2\,\underline{K}_f / \omega_{\max}\right]$, where $\omega_{\max}$ is the largest modeling frequency. Such scaling of the parameters allows sampling the ranges around the characteristic levels of viscosity and Darcy friction. Negative signs of the matrix elements $-\eta_3$ are suggested by the expectation that viscous coupling between the rock and its pore fluid should be reduced when they move in the same direction (analogous to the negative elastic coupling in relation 7). Cases with $\det \underline{\boldsymbol{\eta}}_K < 0$ are rejected from the modeling, as required by the positive definite nature of all constitutive matrices (Part I).

The quality of fitting the phase-velocity and $Q$ data predicted by detailed

modeling of the layered structure is measured by an $L_1$ norm evaluated for the logarithms of the complex wavenumbers $k^*$ for both 'fast' and 'slow' modes:

$$\Phi = \int \left( \left| \ln k^*_{fast} - \ln k^*_{fast\ \mathrm{Data}} \right| + \left| \ln k^*_{slow} - \ln k^*_{slow\ \mathrm{Data}} \right| \right) d\left( \ln \omega \right). \tag{19}$$

Here, $k^*_{fast\ \mathrm{Data}}$ and $k^*_{slow\ \mathrm{Data}}$ are the wavenumbers modeled within the layered structure (Figure 2), and $k^*_{fast}$ and $k^*_{slow}$ are the wavenumbers within the uniform effective medium. Using $\ln k^*$ in the above objective function allows treating the real and imaginary parts of $k^*$ symmetrically and also equalizes the contributions from the two modes, for which the absolute values $|k^*|$ differ by several orders of magnitude. Using $d(\ln\omega)$ boosts the sampling of the low-frequency part of the spectrum during integration, similar to the visual presentation in Figure 2. Note that in the expression 19, the values of $k^*$ can be replaced with complex phase velocities $V^*_{\mathrm{phase}} \equiv \omega / k^*$, and therefore fitting by using norm 19 can also be viewed as fitting $\ln V_{\mathrm{phase}}$ and $Q^{-1}$ simultaneously.

By testing $5 \cdot 10^5$ random combinations of the four variables above, we obtain a solution minimizing the objective function $\Phi$ (Table 2). The velocity dispersion and attenuation curves predicted by such GLS rheology are shown by dashed lines in Figure 2. As seen from this Figure, both the velocities and attenuation are fit reasonably closely, although some deviations still remain. Most importantly, *both* the 'fast' and 'slow' P-wave modes are reproduced by the GLS model.

**Band-limited near-constant *Q*(*f*)**

In this section, we consider another type of "effective" medium, i.e. a medium in which the possibly complex microstructural interactions are replaced with an equivalent GLS model. This model is broadly used to implement a band-limited near-constant *Q* for seismic waves, such as in finite-difference simulations (Zhu et al., 2013). Media with prescribed *Q*(*f*) spectra are typically implemented by mathematical models equivalent to the Generalized Standard Linear Solid (GSLS; Figure 4). As shown in Part I, the GSLS represents a special case of the GLS given by the following relations (equation 37 in Part I):

$$\mathbf{\rho} = \begin{bmatrix} \rho & 0 & \cdots & 0 \\ 0 & 0 & \ddots & \vdots \\ \vdots & \ddots & \ddots & 0 \\ 0 & \cdots & 0 & 0 \end{bmatrix}, \ \mathbf{M} = \begin{bmatrix} \sum_{J=1}^{N} M_J & -M_2 & \cdots & -M_N \\ -M_2 & M_2 & 0 & 0 \\ \vdots & 0 & \ddots & 0 \\ -M_N & 0 & 0 & M_N \end{bmatrix}, \ \mathbf{\eta} = \begin{bmatrix} \eta_1 & 0 & \cdots & 0 \\ 0 & \eta_2 & 0 & 0 \\ \vdots & 0 & \ddots & 0 \\ 0 & 0 & 0 & \eta_N \end{bmatrix}, \tag{20}$$

and $\mathbf{d} = \mathbf{0}$. The moduli $M_J$ and viscosities $\eta_J$ of the Maxwell-solid chains (Figure 4) are selected to form the desired spectrum of relaxation times (Liu et al., 1976). The structure of parameterization 20 is specific and leads to a peculiar character of the wave mode spectrum. For example, with five Maxwell's bodies (*i.e.*, the total number of variables

$N = 6$) with parameters shown in Table 3, the eigenvalue problem in equation 2 yields only one nonzero eigenvalue. The resulting phase velocity and $Q^{-1}$ spectra are of the well-known shapes shown in Figure 5.

In contrast to the primary mode (Figure 5), the remaining five eigenmodes of the GSLS have zero eigenvalues, which are caused by zero mass densities assigned to the internal variables (white circles in Figure 4 and matrix $\boldsymbol{\rho}$ in equation 2). Zero densities mean that the kinetic energy for the internal variables is identically zero, which causes them to behave as 'memory variables', *i.e*. be uniquely expressed through the preceding history of the observed strain (Deng and Morozov, 2013). However, if we seek some physical phenomena occurring behind this memory process, massless variables appear highly problematic. Real physical processes always possess kinetic energy. It is therefore interesting to check how an introduction of small densities for the internal variables would affect the predicted dispersion and $Q^{-1}$ spectra.

The GSLS model contains a relatively large number of internal variables connected in a specific pattern with most coupling parameters set to zero (relations 20). This model can be altered in many ways. To illustrate the effects of internal density, we only try adding equal diagonal elements to the density matrix: $\rho_{JJ} = a\rho_1$, where $a \ll 1$ and $J = 2 \ldots N$. For $a > 0$, additional P-wave modes appear. Similarly to the poroelastic case, we can identify the primary P-wave mode with the one having the largest 'observable' displacement $u_1$. The near-constant spectra of $Q^{-1}(f)$ for the primary mode are achieved by progressive 'freezing', with increasing frequency, of the internal variables containing lower damping factors (Table 3). This freezing increases the attenuation at frequencies $\omega_J = \eta_J / M_J$ (Figures 6a and c).

There exists an important dividing case $a = a_0$ for which the ratios of the moduli to the densities are equal in all Maxwell's bodies: $M_1/\rho = M_J/\rho_J\big|_{J=2,\ldots,N}$ (Figure 4). In this case, the internal variables are not excited by the primary wave, and the wave is nondispersive and attenuation-free. For the GSLS with parameters given in Table 3, this case corresponds to $a_0 = 0.015$. Note that this is a relatively small value of the order of the dissipation rate ($Q^{-1}$) of the original GSLS.

For values of $a$ below and above $a_0$, the effects of density are different. For $a < a_0$, $Q^{-1}(f)$ of the primary mode is near-constant and decreases with $a$, and the velocity dispersion is positive. The secondary modes in this case are faster than the primary $V_{\text{phase}}$, as suggested by their larger $M_J/\rho_J$ ratios. This case is illustrated by selecting $a = 0.01$ in Figures 6a and b. For $a > a_0$, the $Q^{-1}(f)$ increases with $a$, the dispersion is negative, as shown for $a = 0.05$ in Figures 6c and d. In this case, the secondary modes are slower than $V_{\text{phase}}$. Note that the increase of the phase velocity with frequency does not automatically follow from a band-limited near-constant $Q^{-1}(f)$, as it is often thought (Figure 6d). The low-frequency asymptotes of phase velocities in all models are reduced because of the net increases of their densities, and the levels of $Q^{-1}$ for the primary mode vary by 2–3 times. However, these variations can be corrected by adjusting the values of $\rho_1$, $M_J$, and/or $\eta_J$ (Table 3).

With no physical argument for the internal ('memory') variables as well as for their densities, damping factors, and moduli, it is of course impossible to say which of the above internal-density models is correct or more realistic. In terms of achieving a desired $Q^{-1}(\omega)$ spectrum for the primary mode within the ~0.01–1000 Hz frequency band, all of these models are practically equivalent. Observations of secondary P-wave modes near velocity/density contrasts would certainly be a criterion of validity for such models. However, to perform such observations, physical meanings need again to be assigned to the internal variables and the corresponding measurement procedures need to be designed.

From the theoretical point of view, multiple internal variables with zero densities in the GSLS model appear extremely unrealistic. The poroelastic model (Part I) and our WIFF model (Table 2) shows that the internal variables should unlikely be so decoupled. Models of linear solids were originally designed to explain quasi-static lab experiments (Lakes, 2009), in which the density effects are insignificant and cannot be assessed. However, the quasi-static limit is inappropriate for seismic waves, in which the effect of inertia is intertwined with the elastic and frictional ones (equation 2). The selection of sparse matrices $\mathbf{M}$ and $\boldsymbol{\eta}$ with $\mathbf{d} = \mathbf{0}$ in GSLS equations 20 is done only for mathematical convenience, and similar spectra of $Q^{-1}(f)$ could likely be achieved with fuller-rank matrices. Thus, the GSLS may be an oversimplified physically but overly mathematical way to model seismic attenuation. It remains an open question how well this model reproduces the actual processes of wave propagation.

### *Discussion*

With the use of the GLS formulation, the emphasis in analyzing the wave-attenuation phenomena is shifted from constructing empirical parameters and conventions to looking for physical properties. The properties of the medium (the elastic moduli, viscosity and factors of Darcy friction) become matrix and mutually independent. These properties also become differentiated from those of the waves and oscillations, such as the phase velocities and $Q$. Replacing empirical frequency-dependent parameters with models based on differential equations and variational principles allows closer insights into the physical natures of the fluid-flow and internal-friction phenomena.

The most important practical observation from the examples in this paper is that the models of effective media need to explain not only the primary but *multiple* P-wave modes. Only by including both primary and secondary waves it is possible to predict seismic reflectivity or to model lab tests with rocks containing pore fluids. In the traditional viscoelastic approach, we can course construct an individual effective modulus for each of these modes. However, even with frequency-dependent moduli defined for all wave modes, the viscoelastic model does not specify how these moduli should interact to produce a seismic reflectivity from a boundary. By contrast, the GLS model contains all possible interactions in the fairly simple functional forms of the Lagrangian and dissipation functions (equations 1), and all observed effects are predicted from these forms.

The GLS relations 1 are based on only four general principles: 1) the system is mechanical, i.e. governed by the principles of energy and energy dissipation; 2) all interactions are linear, i.e., the governing $L$ and $D$ functions are quadratic; 3) the medium is isotropic; and 4) bulk and shear deformations are not coupled. Note that principles 2) – 4) can readily be relaxed. These principles are also present in most physics-based models of wave propagation. Therefore, it is likely that GLS formulations should be possible for most existing models. The examples of poroelasticity (Appendix A) and WIFF in layered structures and GSLS above show how these formulations are obtained from the microstructure.

There also exist several areas in which the simple GLS model considered here requires extensions: 1) the (arguable) need for viscoelastic (integro-differential in time) operators in the equations of motion, 2) dynamic (i.e., frequency-dependent) properties, in particular viscosity and permeability (Biot, 1962; Johnson et al., 1987), 3) fluid substitution and mixing laws for specific solid/solid and solid/fluid compounds, 4) effects of temperature, thermal flows, and 'thermal waves' (Landau and Lifshitz, 1986) occurring during deformation, 5) effects of surface tension and capillary forces, particularly in cases of multiple and partial fluid saturation, and 6) specific effects in heavy oils and bitumen, in which the viscosity effects likely dominate the 'poroelastic' ones and may be nonlinear. Although these topics require extensive studies, they all fit within the general concept of internal variables and Lagrangian approach of the described framework.

## *Conclusions*

To model wave propagation in a macroscopically-heterogeneous medium, such as seismic reflectivity or measurements with rock samples in the lab, it is important to take into account not only the primary but also the secondary wave modes. Secondary modes occur in the (common) cases of wave-induced fluid flows (WIFF) within porous, grainy, or fractured rock. In such cases, the conventional viscoelastic modulus is generally insufficient for representing the mechanical properties of the medium. The General Linear Solid (GLS) framework described in Part I of this paper is appropriate for this purpose.

In this Part II, the GLS model is used to construct two types of effective media. First, for a rock consisting of alternating thin sandstone layers saturated with brine and gas, the effective medium is 'poro-viscoelastic', i.e. possesses both Darcy's pore-friction and viscosity properties. However, the effective-medium relations can be derived in a (relatively) closed form for the density and elasticity, but not for the parameters of internal friction. The GLS effective medium predicts the velocity dispersion and attenuation for both the primary and secondary P waves. The effective density, moduli, and the properties responsible for internal friction are $2\times2$ matrix quantities. Notably, the effective elastic bulk modulus (responsible for the low-frequency P-wave velocity) is significantly lower than the lower-bound (Reuss) average of the moduli of the constituent rocks. This modulus reduction occurs because of the WIFF effect, consisting in the fluid

flowing across the layer boundaries. If the layers are insulated, the effective modulus matches the Reuss average and the wave attenuation is extremely low.

In the second example, an effective medium equivalent to the broadly used Generalized Standard Linear Solid (GSLS) is considered. The GSLS appears to be a specific mathematical system with many but weakly connected internal variables. The physical, GLS point of view suggests considering the inertial effects and interactions between the variables involved in the GSLS. Such inertial effects again lead to secondary wave modes with complex dispersion characteristics.

### *Acknowledgments*

W. D. was supported by the Scholarship Council, P. R. China. GNU Octave software (http://www.gnu.org/software/octave/) was used for numerical modeling. GMT programs (Wessel and Smith, 1995) were used for preparing illustrations.

### *References*

Biot, M. A. 1962. Mechanics of deformation and acoustic propagation in porous media, J. Appl. Phys. 23, 1482–1498.

Bourbié, T., Coussy, O., and Zinsiger, B. 1987. *Acoustics of porous media*, Editions TECHNIP, France, ISBN 2-7108-0516-2

Carcione, J. M., and S. Picotti, 2006. P-wave seismic attenuation by slow-wave diffusion: Effects of inhomogeneous rock properties, Geophysics, 71 (3), O1–O8, doi: 10.1190/1.2194512

Coulman, T., Deng, W., and Morozov, I., 2013. Models of seismic attenuation measurements in the laboratory, Canadian J. Expl. Geoph, 38 (1), 51–67.

Deng, W., and I. B. Morozov, 2013. New approach to finite-difference memory variables by using Lagrangian Mechanics, CSPG/CSEG/CWLS Convention 2013, Calgary, AB, Canada, May 2013; http://cseg.ca/assets/files/resources/abstracts/2013/243_GC2013_New_Approach_to_Finite-Difference_Memory_Variables.pdf, last accessed on August 18, 2014.

Dutta, N. C., and H. Odé, 1979a. Attenuation and dispersion of compressional waves in fluid-filled porous rocks with partial gas saturation (White model)–Part I: Biot theory, Geophysics, 44 (11), 1777–1788.

Dutta, N. C., and H. Odé, 1979b. Attenuation and dispersion of compressional waves in fluid-filled porous rocks with partial gas saturation (White model)–Part II: Results, Geophysics, 44 (11), 1789–1805.

Gurevich, B., Zyirianov, and S. L. Lopatnikov, 1997. Seismic attenuation in finely layered porous rocks: Effects of fluid flow and scattering, Geophysics, 62 (1), 319–324.

Johnson, D. L., J. Koplik, and R. Dashen, 1987. Theory of dynamic permeability and tortuosity in fluid-saturated porous media, J. Fluid Mech., **176**, 379–402.

Lakes, R., 2009. *Viscoelastic materials*, Cambridge, ISBN 978-0-521-88568-3.

Landau L. D., and Lifshitz, E.M., 1986. Course of theoretical physics, volume 7 (3rd

English edition): Theory of elasticity, Butterworth-Heinemann, ISBN 978-0-7506-2633-0

Liu, H. P., Anderson, D. L., and Kanamori, H., 1976. Velocity dispersion due to anelasticity: implications for seismology and mantle composition, Geophys. J. R. Astr. Soc., 47, 41–58.

Makarynska, D., B. Gurevich, J. Behura, and M. Batzle, 2010. Fluid substitution in rocks saturated with viscoelastic fluids, Geophysics, **75** (2), E115–E122, doi:10.1190/13360313.

Mavko, G. 2013. Relaxation shift in rocks containing viscoelastic pore fluids, Geophysics, 78; P. M19-M28, doi: 10.1190/GEO2012-0272.1

Morozov, I. B. and W. Deng, submitted to Geophysics, Unified macroscopic model for viscoelasticity and wave-induced flow – Part I: General Linear Solid.

Müller, T., B. Gurevich, and M. Lebedev, 2010. Seismic wave attenuation and dispersion resulting from wave-induced flow in porous rock – A review, *Geophysics* **75**, 75A147 – 75A164.

Wessel, P., and Smith, W. H. F., 1995. New version of the Generic Mapping Tools released, EOS, Trans. Am. Geophys. Union **76**, 329.

White, J. E., 1975. Computed seismic speeds and attenuation in rocks with partial gas saturation, Geophysics, **40** (2), 224–232.

Zhu, T., J. M. Carcione, and J.M. Harris, 2013, Approximating constant-Q seismic propagation in the time domain: Geophysical Prospecting, **61**, 931 – 940, doi: 10.1111/1365-2478.12044.

### *Figure captions*

Figure 1. Layered sequence of alternating brine- and gas -saturated sandstone layers. The inset shows two types of boundary conditions for fluid content.

Figure 2. Characteristics of effective P-wave in a finely layered poroelastic medium (Table 1): a) velocity dispersion, b) attenuation. Black and red lines and coordinate axes show the 'fast' and 'slow' modes, respectively. Dashed lines show the predictions by the effective-medium GLS model. In plot a), the effective velocity in a structure with insulated layers is also shown.

Figure 3. Amplitudes of the wave modes within the brine-saturated (solid lines) and gas-saturated (dashed lines) layers in Figure 1, relative to the amplitude of the effective wave, for two cases: a) 'fast' effective wave mode, and b) 'slow' effective wave. Labels 'brine' and 'gas' refer to brine- and gas-saturated layers, and arrows '→' and '←' indicate the forward- and backward-propagating modes, respectively. Black lines and coordinate axes indicate the displacements of the saturated rock, and red lines are the variations of fluid content.

Figure 4. Effects of the proportion of gas-saturated rock in the periodic-layering model (Figure 1), as functions of the fraction of gas-bearing layers: a) Velocities of effective fast and slow waves; b) Parameter $\alpha$ in equation 7.

Figure 4. Generalized Standard Linear Solid commonly used in finite-difference modeling of seismic waves in viscoelastic media. Variable $u_1$ and its gradients $\varepsilon_1$ represent the observable rock deformation, and variables $u_J$ ($J = 2..N$) are the internal variables added to implement band-limited attenuation (Liu et al., 1976).

Figure 5. Characteristics of a plane P wave in a GSLS medium (Table 3): a) attenuation, b) phase velocity.

Figure 6. Propagation of a plane P wave in a GSLS medium with densities assigned to the internal variables: a) attenuation for internal density levels of 1% of the main density (Table 3), b) phase velocity for 1% internal densities, c) and d) – the same for 5% internal densities (Table 3). The numbers of the wave modes are labeled. Black lines indicate the primary mode, and gray lines are the additional modes

due to the internal densities.

## *Tables*

Table 1. Parameters of alternating layers in the 1-D WIFF modeling (Figure 1; Dutta and Odé, 1979b)

| | | |
|---|---|---|
| **Layering** | | |
| $H_1 = H_2$ | 0.01 m | Layer thickness |
| **Rock** | | |
| $V_P$ | 1500 m/s | P-wave velocity of dry matrix |
| $V_S$ | 1000 m/s | S-wave velocity of dry matrix |
| $K_s$ | 35 GPa | Bulk modulus of solid grains |
| $\rho_s$ | 2650 kg/m$^3$ | Density of solid grains |
| $\phi$ | 0.3 | Porosity |
| $\kappa$ | $9.869233 \cdot 10^{-13}$ m$^2$ (1 Darcy) | Permeability |
| $a$ | 1 | Tortuosity of pore space |
| **Brine** | | |
| $K_{fl}$ | 2.4 GPa | Bulk modulus |
| $\rho_{fl}$ | 1000 kg/m$^3$ | Density |
| $\eta$ | $1 \cdot 10^{-3}$ | Viscosity |
| **Gas** | | |
| $K_{fl}$ | 0.0022 GPa | Bulk modulus |
| $\rho_{fl}$ | 100 kg/m$^3$ | Density |
| $\eta$ | $1.5 \cdot 10^{-5}$ | Viscosity |

Table 2. Physical parameters of the effective medium

| *Parameter* | *Value* |
|---|---|
| $\rho$ | 1887 g/cm$^3$ |
| $\rho_f$ | 101 g/cm$^3$ |
| $\underline{K}_f$ | 1.82 GPa |
| $\underline{\beta}$ | 0.95 |
| $\underline{M}$ | 1.45 GPa |
| $\underline{\mu}$ | 1.85 GPa |
| $\eta_1$ [1] | 5642 Pa·s |
| $\eta_2$ [1] | 5667 Pa·s |
| $\eta_3$ [1] | 5371 Pa·s |
| $d$ [2] | 0.51·GPa·s/m$^2$ |

[1]) Equation 18.

[2]) Equation 17.

Table 3. Parameters of the Generalized Standard Linear Solid (GSLS) medium

| | | | GSLS model (Figure 5a, b) | GSLS with 1% (5%) internal densities (Figure 5c, d) |
|---|---|---|---|---|
| $J$ | $M_J$, (GPa) | $\eta_J$ (Pa·s) | $\rho_J$ (kg/m$^3$) | $\rho_J$ (kg/m$^3$) |
| 1 | 10 | 0 | 2000 | 2000 |
| 2 | 0.15 | $9.3\cdot10^8$ | 0 | 20 (100) |
| 3 | 0.15 | $9.3\cdot10^7$ | 0 | 20 (100) |
| 4 | 0.15 | $9.3\cdot10^6$ | 0 | 20 (100) |
| 5 | 0.15 | $9.3\cdot10^5$ | 0 | 20 (100) |
| 6 | 0.15 | $9.3\cdot10^4$ | 0 | 20 (100) |

***Figures***

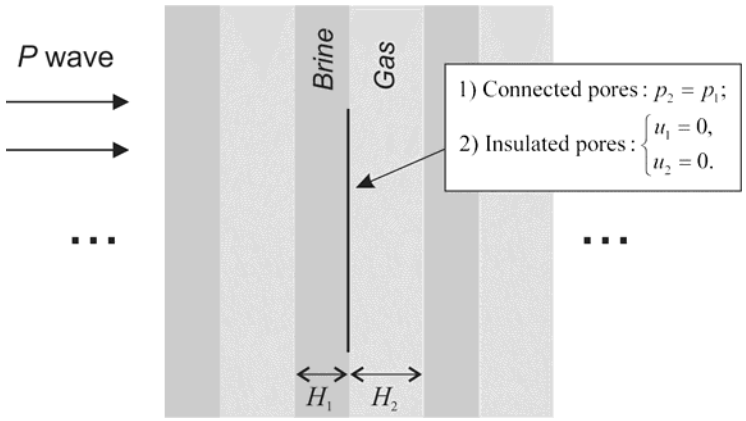


Figure 1. Layered sequence of alternating brine- and gas -saturated sandstone layers. The inset shows two types of boundary conditions for fluid content.

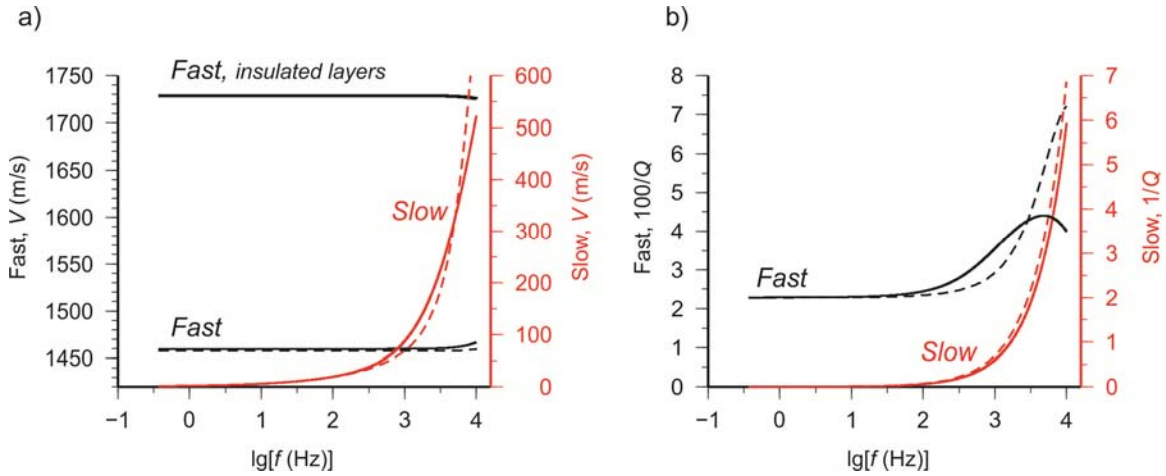


Figure 2. Characteristics of effective P-wave in a finely layered poroelastic medium (Table 1): a) velocity dispersion, b) attenuation. Black and red lines and coordinate axes show the 'fast' and 'slow' modes, respectively. Dashed lines show the predictions by the effective-medium GLS model. In plot a), the effective velocity in a structure with insulated layers is also shown.

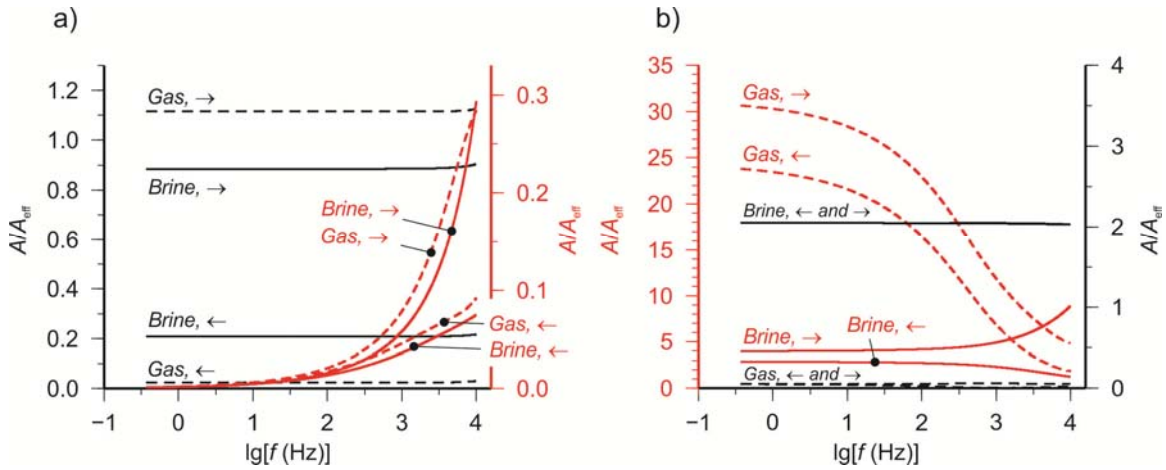


Figure 3. Amplitudes of the wave modes within the brine-saturated (solid lines) and gas-saturated (dashed lines) layers in Figure 1, relative to the amplitude of the effective wave, for two cases: a) 'fast' effective wave mode, and b) 'slow' effective wave. Labels 'brine' and 'gas' refer to brine- and gas-saturated layers, and arrows '→' and '←' indicate the forward- and backward-propagating modes, respectively. Black lines and coordinate axes indicate the displacements of the saturated rock, and red lines are the variations of fluid content.

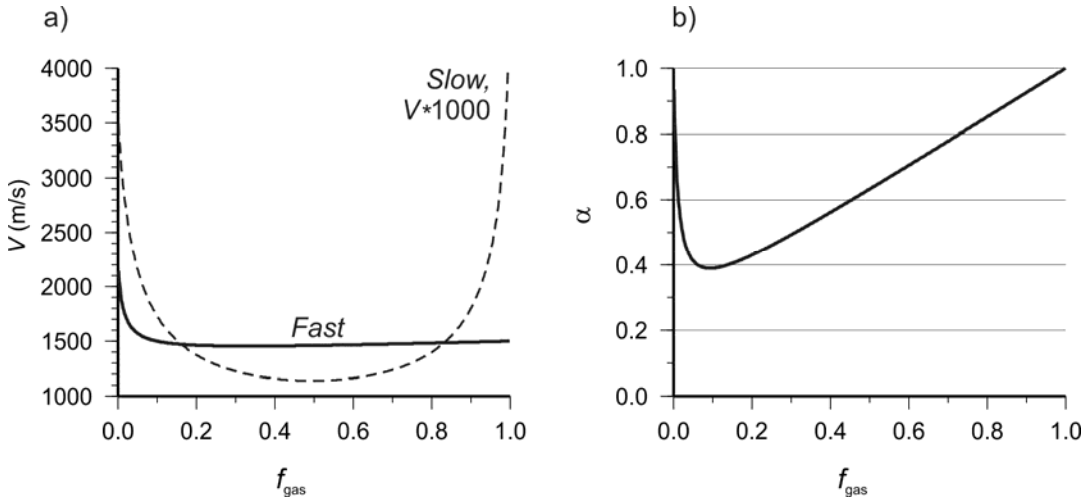


Figure 4. Effects of the proportion of gas-saturated rock in the periodic-layering model (Figure 1), as functions of the fraction of gas-bearing layers: a) Velocities of effective fast and slow waves; b) Parameter $\alpha$ in equation 7.

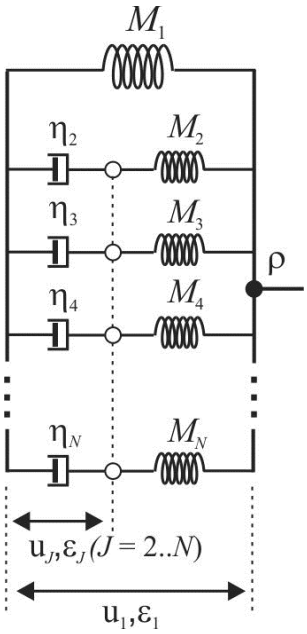


Figure 4. Generalized Standard Linear Solid commonly used in finite-difference modeling of seismic waves in viscoelastic media. Variable $u_1$ and its gradients $\varepsilon_1$ represent the observable rock deformation, and variables $u_J$ ($J = 2..N$) are the internal variables added to implement band-limited attenuation (Liu et al., 1976).

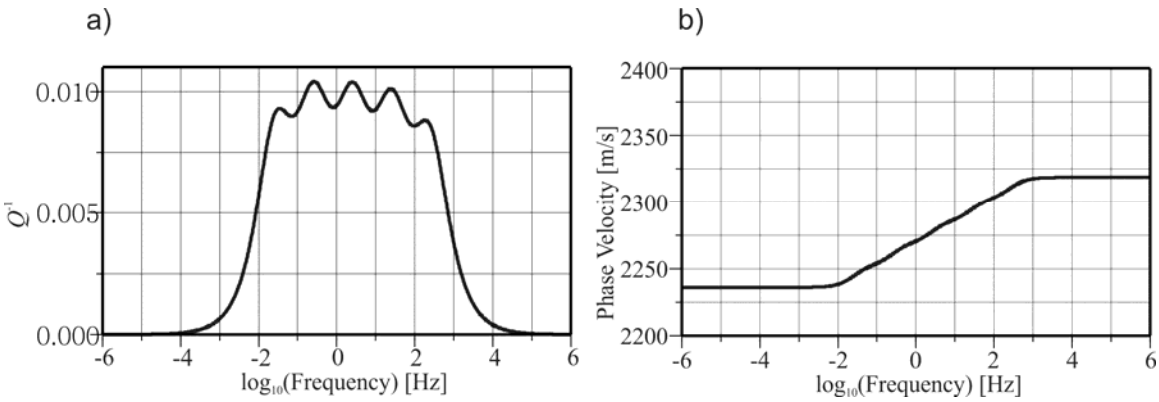


Figure 5. Characteristics of a plane P wave in a GSLS medium (Table 3): a) attenuation, b) phase velocity.

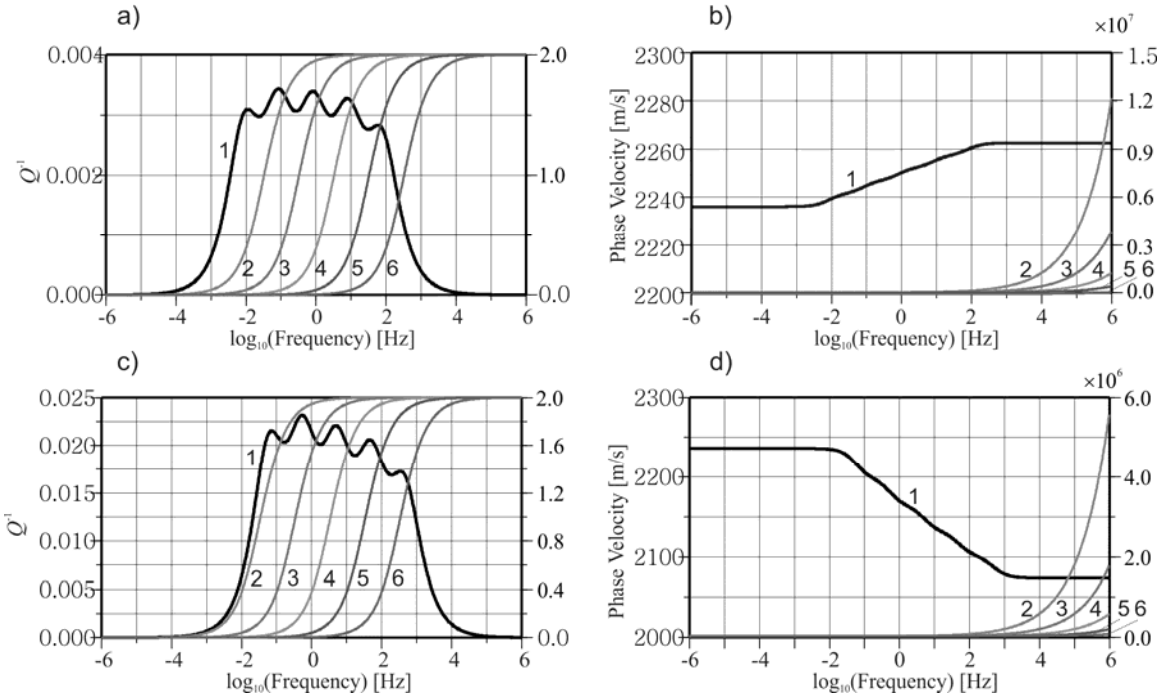


Figure 6. Propagation of a plane P wave in a GSLS medium with densities assigned to the internal variables: a) attenuation for internal density levels of 1% of the main density (Table 3), b) phase velocity for 1% internal densities, c) and d) – the same for 5% internal densities (Table 3). The numbers of the wave modes are labeled. Black lines indicate the primary mode, and gray lines are the additional modes due to the internal densities.

## *Appendix A: Effective-medium parameter matrices for poroelasticity*

In poroelasticity (Biot, 1962), the microstructural model consists of a fluid with density $\rho_f$ and bulk modulus $K_{fl}$ saturating porosity $\phi$ in a solid matrix with density $\rho_s$ and bulk modulus $K_s$. In this Appendix, we show how the effective 2×2 density and bulk-modulus matrices are obtained from this microstructural model by preserving the kinetic and elastic-energy terms in the Lagrangian (equation 1). Consideration of the elastic energy also provides the Gassmann's fluid substitution equation. The parameters of the effective GLS medium are obtained by considering several independent deformations and requiring that the kinetic and elastic energies of the effective medium equal those of the microstructure in all cases.

### Density

The density matrix for the effective poroelastic medium is (equation 32 in Part I):

$$\boldsymbol{\rho} = \begin{bmatrix} \rho & -\rho_f \\ -\rho_f & \dfrac{a}{\phi}\rho_f \end{bmatrix}, \tag{A1}$$

where $\rho$ is the mass density of the effective medium and $a \geq 1$ is the tortuosity of the pore space. The meanings of these quantities are determined later in this paragraph. This matrix can also be obtained by considering a (hypothetical) experiment of applying arbitrary velocities to the rock and fluid phases and measuring the kinetic energy. The fluid velocity equals $\mathbf{v}_{\text{fluid}} = \mathbf{v}_1 - \left(\mathbf{v}_2 + \mathbf{v}_r\right)/\phi$, where $\mathbf{v}_\perp$ denotes the random component of fluid velocity added to the local macroscopic flow $\mathbf{v}_2$ (Part I). For this random velocity, $\langle \mathbf{v}_r \rangle = \mathbf{0}$. The average magnitude of $\mathbf{v}_r$ is proportional to $\mathbf{v}_2$ and dependent on the structure of the pore space, and therefore we can define the tortuosity parameter *a* so that $\mathbf{v}_2^2 + \langle \mathbf{v}_r^2 \rangle = a\mathbf{v}_2^2$. Note that from this relation, $a \geq 1$. Therefore, the average kinetic energy density for mutually independent $\mathbf{v}_1$ and $\mathbf{v}_2$ is:

$$\langle E_{kin} \rangle = \frac{\rho_s}{2}(1-\phi)\mathbf{v}_s^2 + \frac{\rho_f}{2}\phi\mathbf{v}_f^2 = \frac{\rho}{2}\mathbf{v}_1^2 - \rho_f \mathbf{v}_1\mathbf{v}_2 + \frac{a}{2\phi}\rho_f \mathbf{v}_2^2, \tag{A2}$$

where $\rho \equiv \rho_s(1-\phi) + \rho_f\phi$. This expression can be compactly written as a quadratic form based on the effective-medium density matrix $\boldsymbol{\rho}$ in equation A1:

$$\langle E_{kin} \rangle = \frac{1}{2}\dot{\mathbf{u}}^T \boldsymbol{\rho} \dot{\mathbf{u}}, \tag{A3}$$

where $\dot{\mathbf{u}} \equiv \begin{pmatrix} \mathbf{v}_1 & \mathbf{v}_2 \end{pmatrix}^T$.

## Bulk modulus

To derive the effective bulk modulus matrix, we use the standard selection of variables $\Delta \equiv \mathrm{tr}\,\varepsilon$ and $\xi \equiv -\mathrm{div}\,\mathbf{w}$, where $\varepsilon$ is the observable strain of the material and $\mathbf{w}$ is the filtration velocity (Part I). With such parameterization, the dilatation of the solid and fluid phases within the specimen are:

$$\begin{pmatrix} \Delta_s \\ \Delta_{fl} \end{pmatrix} = \mathbf{U} \begin{pmatrix} \Delta \\ \xi \end{pmatrix}, \tag{A4}$$

where the matrix $\mathbf{U}$ relates these macroscopic field variables and microstructural parameters $\Delta_s$ and $\Delta_{fl}$:

$$\mathbf{U} = \begin{bmatrix} 1 & -1 \\ 1 & -1/\phi \end{bmatrix}. \tag{A5}$$

The elastic property of the material is given in the GLS model by potential function $V$ (quadratic form similar to A3; equation 6 in Part I):

$$V = \frac{1}{2}\boldsymbol{\Delta}^T \mathbf{K} \boldsymbol{\Delta} - \tilde{\boldsymbol{\varepsilon}}_{ij}^T \boldsymbol{\mu} \tilde{\boldsymbol{\varepsilon}}_{ij}, \tag{A6}$$

where the matrix $\mathbf{K}$ equals for poroelasticity (equation 29 in Part I):

$$\mathbf{K} = \begin{bmatrix} K_f & -\beta M \\ -\beta M & M \end{bmatrix}. \tag{A7}$$

and the corresponding compliance (equation 30 in Part I):

$$\mathbf{J} = \mathbf{K}^{-1} = \frac{1}{K_0} \begin{bmatrix} 1 & \beta \\ \beta & K_f / M \end{bmatrix}, \tag{A8}$$

where $K_0 = K_f - \beta^2 M$. The parameters of these matrices can be obtained by considering the variations of the closed-system potential A6 and its open-system counterpart (compliance A8; see equation 14 in Part I) in several experiments. This derivation follows Bourbié *et al*. (1987) in a simplified matrix form that can be readily extended to more complex GLS systems.

In the first experiment, consider the system statically compressed with no fluid flow allowed ($\xi = 0$; closed system). This experiment simply corresponds to the measurement of the 'wet' bulk modulus in a jacketed specimen by applying an averaged deformation $\Delta$. In this case, the double elastic energy density (equation A6) equals $2V = \boldsymbol{\Delta}^T \mathbf{K} \boldsymbol{\Delta} = K_f \Delta^2$, showing that $K_f$ in relations A6 and A8 is the measured 'wet' modulus.

In the second experiment, consider drained rock with zero pore pressure under confining stress $\bar{\sigma}$. The macroscopic deformation is given by relation A8

$$\begin{pmatrix} \Delta \\ \xi \end{pmatrix} = \mathbf{J} \begin{pmatrix} \bar{\sigma} \\ 0 \end{pmatrix} = \frac{\bar{\sigma}}{K_0} , \tag{A9}$$

showing that $K_0$ is the modulus of the drained rock. From relation A4, the strains of the two phases equal:

$$\begin{pmatrix} \Delta_s \\ \Delta_{fl} \end{pmatrix} = \mathbf{U} \begin{pmatrix} \Delta \\ \xi \end{pmatrix} = \bar{\sigma} K_0^{-1} \begin{pmatrix} 1-\beta \\ 1-\beta/\phi \end{pmatrix} . \tag{A10}$$

The entire deformation and strain energy in this system belongs to the solid, and consequently $\Delta_s = \bar{\sigma} K_s^{-1}$. Therefore, the (measurable) compliance of solid grains equals $K_s^{-1} = K_0^{-1}(1-\beta)$. As a result, quantity $\beta$ in expressions A7 and A8 represents the ratio of the dry and solid-grain moduli:

$$\beta = 1 - K_0 / K_s . \tag{A11}$$

In the third experiment, consider the rock matrix and fluid at equilibrium, with both the confining and pore pressures held equal *p*. The deformation of the two phases is:

$$\begin{pmatrix} \Delta_s \\ \Delta_{fl} \end{pmatrix} = \mathbf{UJ} \begin{pmatrix} -3p \\ 3p \end{pmatrix} = 3pK_0^{-1} \begin{pmatrix} 2\beta - K_f/M - 1 \\ \beta - K_f/(\phi M) - 1 + \beta/\phi \end{pmatrix} . \tag{A12}$$

The volumetric strain within the fluid should satisfy $\Delta_{fl} = -3pK_{fl}^{-1}$, and after some simplification, we obtain: $\phi K_{fl}^{-1} = M^{-1} - K_s^{-1}(\beta - \phi)$. Therefore, the elastic coupling *M* in relation A7 can be determined from the following average of the compliances of the solid and fluid phases: $M^{-1} = K_s^{-1}(\beta - \phi) + \phi K_{fl}^{-1}$. By using this relation, the above equation $K_f = K_0 + \beta^2 M$ (which can be written as $(K_f - K_0)^{-1} = M^{-1}/\beta^2$) yields several forms of Gassmann's equation for the 'wet' modulus $K_f$; for example (Bourbié *et al.*, 1987):

$$K_f^{-1} = \frac{\phi K_0^{-1}\left(K_s^{-1} - K_{fl}^{-1}\right) + K_s^{-1}\left(K_s^{-1} - K_0^{-1}\right)}{\phi\left(K_s^{-1} - K_{fl}^{-1}\right) + \left(K_s^{-1} - K_0^{-1}\right)} . \tag{A13}$$

### *Appendix B: Propagator method for layers with sealed boundaries*

In this Appendix, we give a modification of the propagator method for modeling the wavefield in a finely layered structure (equations 38–42 in Part I). In the present case, we treat the boundaries of the layers as impermeable for pore fluids. In contrast to the case considered in Part I, pore pressures within the brine- and gas-saturated layers are different, but the relative fluid displacements $u_2$ are zero on both sides of the boundary (the second type of boundary condition in the inset of Figure 1).

As in Part I, let us parameterize the wavefield within any layer by a four-component vector $\mathbf{q}_r = \left(A_1^+ \quad A_2^+ \quad A_1^- \quad A_2^-\right)^T$, where $A_J^\pm$ are the amplitudes of the forward- and backward-traveling modes. At an arbitrary coordinate $x$ within the layer, the wavefield is

$$\mathbf{q}(x) = \mathbf{P}(x)\mathbf{q}_r, \tag{B1}$$

where

$$\mathbf{P}(x) = \begin{bmatrix} e^{ik_1 x} & 0 & 0 & 0 \\ 0 & e^{ik_2 x} & 0 & 0 \\ 0 & 0 & e^{-ik_1 x} & 0 \\ 0 & 0 & 0 & e^{-ik_2 x} \end{bmatrix}. \tag{B2}$$

The displacement in this field is given by applying an additional matrix $\mathbf{U}$: $\mathbf{U}\mathbf{q}(x) = \mathbf{U}\mathbf{P}(x)\mathbf{q}_r$ (equation 39 in Part I). Using this matrix, the boundary conditions $u_2(x = 0) = u_2(x = H)$ ($H$ is the thickness of the layer) can be combined in a matrix equation:

$$\begin{bmatrix} \underline{\mathbf{U}\mathbf{P}(0)}_2 \\ \underline{\mathbf{U}\mathbf{P}(H)}_2 \end{bmatrix} \mathbf{q}_r = \begin{pmatrix} 0 \\ 0 \end{pmatrix}, \tag{B3}$$

where the notation $\underline{\mathbf{A}}_j$ denotes the $j$-th row of matrix $\mathbf{A}$ (note that $\mathbf{P}(0) \equiv \mathbf{I}$). The equations B3 can be partitioned separating the contributions from the 'fast' (subscript 1) and 'slow' modes (subscript 2):

$$\mathbf{U}_1\mathbf{q}_{r1} + \mathbf{U}_2\mathbf{q}_{r2} = \begin{pmatrix} 0 \\ 0 \end{pmatrix}, \tag{B4}$$

where vectors $\mathbf{q}_{r1}$ and $\mathbf{q}_{r2}$ are: $\mathbf{q}_{r1,2} \equiv \begin{pmatrix} A_{1,2}^+ \\ A_{1,2}^- \end{pmatrix}$. By solving this equation, modes $\mathbf{q}_{r2}$ can be

expressed as $\mathbf{q}_{r2} = \mathbf{Q}\mathbf{q}_{r1}$, where $\mathbf{Q} = -\left(\mathbf{U}_2\right)^{-1}\mathbf{U}_1$. Again combining the 'fast' and 'slow' modes together, the complete wavefield at any point *x* equals:

$$\mathbf{q}\left(x\right) = \mathbf{P}_1\left(x\right)\mathbf{q}_{r1}, \tag{B5}$$

where:

$$\mathbf{P}_1\left(x\right) \equiv \mathbf{P}\left(x\right)\begin{bmatrix} 1 & 0 \\ Q_{11} & Q_{12} \\ 0 & 1 \\ Q_{21} & Q_{22} \end{bmatrix}. \tag{B6}$$

To derive the transformation of the wavefield $\mathbf{q}_r^+$ across a boundary of two layers, we use the boundary condition (equation 41 in Part I):

$$\mathbf{B}^1\mathbf{P}_1^1\left(H_1\right)\mathbf{q}_{r1}^1 = \mathbf{B}^2\mathbf{P}_1^2\left(0\right)\mathbf{q}_{r1}^2, \tag{B7}$$

where the superscripts and subscript in $H_1$ denote the layer numbers. However, in this case, matrices **B** are 2×4 and only contain the conditions for rock displacement and confining stress (the first and third rows of **B** in equation 41 in Part I). Finally, this gives for the field in layer 2:

$$\mathbf{q}_{r1}^2 = \left(\mathbf{B}^2\mathbf{P}_1^2\left(0\right)\right)^{-1}\mathbf{B}^1\mathbf{P}_1^1\left(H_1\right)\mathbf{q}_{r1}^1. \tag{B8}$$

This relation is similar to equation 13. When applied recursively, it allows computing the forward-traveling modes in any layer, and the total wavefield is given by equation B5.